TECHNICAL REPORT ARBRL-TR-02548

A NUMERICAL STUDY OF SHOCK INITIATION OF COMPOSITION-B BY HIGH-SPEED IMPACT OF SMALL STEEL PROJECTILES

Yun K. Huang
John J. Starkenberg
Alvin L. Arbuckle

February 1984

US ARMY ARMAMENT RESEARCH AND DEVELOPMENT CENTER
BALLISTIC RESEARCH LABORATORY
ABERDEEN PROVING GROUND, MARYLAND

Destroy this report when it is no longer needed.
Do not return it to the originator.

Additional copies of this report may be obtained from the National Technical Information Service, U. S. Department of Commerce, Springfield, Virginia 22161.

The findings in this report are not to be construed as an official Department of the Army position, unless so designated by other authorized documents.

The use of trade names or manufacturers' names in this report does not constitute indorsement of any commercial product.

UNCLASSIFIED
SECURITY CLASSIFICATION OF THIS PAGE *(When Data Entered)*

REPORT DOCUMENTATION PAGE		READ INSTRUCTIONS BEFORE COMPLETING FORM
1. REPORT NUMBER TECHNICAL REPORT ARBRL-TR-02548	2. GOVT ACCESSION NO.	3. RECIPIENT'S CATALOG NUMBER
4. TITLE *(and Subtitle)* A NUMERICAL STUDY OF SHOCK INITIATION OF COMPOSITION-B BY HIGH-SPEED IMPACT OF SMALL STEEL PROJECTILES		5. TYPE OF REPORT & PERIOD COVERED Final 6. PERFORMING ORG. REPORT NUMBER
7. AUTHOR*(s)* Y. K. Huang, J. J. Starkenberg, A. L. Arbuckle		8. CONTRACT OR GRANT NUMBER*(s)*
9. PERFORMING ORGANIZATION NAME AND ADDRESS US Army Ballistic Research Laboratory, ARDC ATTN: DRSMC-BLT(A) Aberdeen Proving Ground, MD 21005		10. PROGRAM ELEMENT, PROJECT, TASK AREA & WORK UNIT NUMBERS 1L161102AH43
11. CONTROLLING OFFICE NAME AND ADDRESS US Army AMCCOM, ARDC Ballistic Research Laboratory, ATTN: DRSMC-BLA-S(A) Aberdeen Proving Ground, MD 21005		12. REPORT DATE February 1984 13. NUMBER OF PAGES 41
14. MONITORING AGENCY NAME & ADDRESS*(if different from Controlling Office)*		15. SECURITY CLASS. *(of this report)* UNCLASSIFIED 15e. DECLASSIFICATION/DOWNGRADING SCHEDULE

16. DISTRIBUTION STATEMENT *(of this Report)*

Approved for public release; distribution unlimited.

17. DISTRIBUTION STATEMENT *(of the abstract entered in Block 20, if different from Report)*

18. SUPPLEMENTARY NOTES

19. KEY WORDS *(Continue on reverse side if necessary and identify by block number)*

critical energy criterion
fragment impact
mass detonation
munitions vulnerability
projectile impact
reactive shock waves
shock-to-detonation transition
shock initiation

20. ABSTRACT *(Continue on reverse side if necessary and identify by block number)*

Using the SIN and 2DE computer codes, we have conducted a numerical study of the shock initiation response of both bare and covered composition-B charges to projectile impact. In the bare charge case we observed two modes of shock initiation. Independence of the explosive response with respect to projectile aspect ratio was verified and critical conditions were determined as a function of projectile diameter with unit aspect ratio. The critical velocity was observed to have a linear dependence on the reciprocal of the square root of

DD FORM 1 JAN 73 1473 EDITION OF 1 NOV 65 IS OBSOLETE

UNCLASSIFIED
SECURITY CLASSIFICATION OF THIS PAGE *(When Data Entered)*

20. Abstract (continued)

the diameter with values a little below experimental data. Additional linear relations to completely describe buildup to detonation were generated from the results. We found that development of detonation is similar in the case of covered charges. When the critical velocity was corrected for cover plate thickness, good agreement between the results for bare and covered charges was observed.

TABLE OF CONTENTS

LIST OF ILLUSTRATIONS

LIST OF TABLES

I. INTRODUCTION

Projectile impact shock initiation of high explosive has long been a subject of considerable interest in the energetic materials community. Considerable experimental data has been generated over the years.[1-3] Numerical modeling of projectile impact shock initiation for comparison with experiments has been reported in at least one case.[4] However, a detailed analysis of the flow fields revealed by the computations was not presented.

Accordingly, we consider in this work the problem of composition-B (bare as well as confined) impacted by small high-speed steel projectiles. Using the reactive hydrodynamic codes SIN[5] and 2DE[6] we have addressed the posed problem numerically. This approach is favored by virtue of its simulation capability, detailed results, moderate cost, and lack of risk to the investigator. In the following section, we describe the numerical simulation of projectile impact on bare charges for six different projectile diameters. Results obtained with 2DE for projectile impact are compared with planar impact results obtained using SIN. The results were used to generate linear fits which suffice to describe the impact shock initiation of bare charges consistent with the critical energy criterion.

---

1. *D. C. Slade and J. Dewey, "High-Order Initiation of Two Military Explosives by Projectile Impact," Ballistic Research Laboratory Report No. 1021, July 1957 (AD 145868).*

2. *S. M. Brown and E. G. Whitbread, "The Initiation of Detonation by Shock Waves of Known Duration and Intensity," Les Ondes De Detonation, C.N.R.S. No. 109 (Paris, 1962), pp 69-80.*

3. *L. A. Roslund, J. W. Watt, and N. L. Coleburn, "Initiation of Warhead Explosives by the Impact of Controlled Fragments I. Normal Impact," Naval Ordnance Laboratory Technical Report NOLTR-73-124, August 1974.*

4. *K. L. Bahl, H. C. Vantine and R. C. Wlingort, "The Shock Initiation of Bare and Covered Explosives by Projectile Impact," Seventh Symposium (International) on Detonation, June 1981, pp 325-335.*

5. *C. L. Mader and M. S. Shaw, "Users Manual for SIN, A One-Dimensional Hydrodynamic Code for Problems which Include Chemical Reactions, Elastic Plastic Flow, Spalling Phase Transitions, Melting, Forest Fire, Detonation Buildup, and SESAME Tabular Equation of State," Los Alamos Scientific Laboratory Report LA-7264-M, September 1978.*

6. *J. D. Kershner and C. L. Mader, "2DE, A Two-Dimensional Continuous Eulerian Hydrodynamic Code for Computing Multicomponent Reactive Hydrodynamic Problems," Los Alamos Scientific Laboratory Report LA-4846, March 1972.*

We then turned our attention to a numerical assessment of shock initiation in covered charges. The results show the buildup of shock to detonation in detail by means of contour plots. We also checked our results with the Jacobs-Roslund formula.[3]

II. PROJECTILE IMPACT SHOCK INITIATION OF BARE EXPLOSIVE CHARGES

Geometry and Computational Considerations

In our computations, we have considered steel cylinders of aspect ratio (ℓ/ϕ) equal to one and composition-B charges of aspect ratio one-half. Sufficient target material is provided when the explosive diameter is three times the projectile diameter. This aspect ratio is considered adequate to take account of rarefaction effects from free surfaces and edges. Moreover, Brown and Whitbread[2] show that different aspect ratios, except for the case of a disc ($\ell/\phi < 1/4$), do not result in different critical velocities for shock initiation.

With the considerations mentioned above, we have set up impact problems for 2DE calculations with axisymmetric grids as summarized in Table 1. Here ϕ is the projectile diameter, ΔR the radial cell size, I the number of cells along the radial axis, ΔZ the axial cell size, J the number of cells along the axis of symmetry, ΔT the time step of each computing cycle, and N the total number of cycles to be completed.

TABLE 1

Input Data for 2DE Computational Grids - Bare Charges

ϕ (mm)	ΔR (mm)	I	ΔZ (mm)	J	ΔT (μs)	N
5	0.25	45	0.25	68	0.005	400
8	0.40	45	0.40	68	0.010	350
10	0.50	45	0.50	68	0.010	400
12	0.40	65	0.40	98	0.010	530
15	0.50	65	0.50	98	0.010	530
18	0.60	65	0.60	98	0.015	400

Results

A number of graphical representations of our numerical results are available. The sequence of events in projectile impact shock initiation is most clearly illustrated in the series of mass fraction contour plots of Figure 1a. The mass fraction varies from one to zero as chemical reaction in the explosive runs to completion. The plots show results for impact of a 5 mm diameter projectile at 1.4 mm/μs. The corresponding isobar plots are shown in Figure 1b. Detonation, which may be recognized by the close spacing of the contour lines, is observed to begin at the shock front and spread outward. Similar plots for the 5 mm projectile at a subcritical impact velocity of 1.2 mm/μs are shown in Figures 2a and 2b. In this case, no detonation develops and concentration of the mass fraction contour lines is not observed. Figure 3 shows mass fraction contour plots for a projectile 15 mm in diameter with an impact velocity of 0.7 mm/μs, in which case initiation resulted. In contrast to the small diameter, high velocity case, initiation here first appears after the shock has propagated some distance from the impact point. The ensuing detonation propagates outwards. This latter observation is typical of all the computations for $\phi > 5$ mm.

We also made computations comparing projectiles of different aspect ratio. Mass fraction contour plots for the 1.2 mm/μs impact of a 10 mm diameter projectile with aspect ratios of 1.0 and 1.5 are shown in Figure 4. The results show that the flow fields created in the two cases are essentially identical during the period required for buildup to detonation. Computations were made with impact velocity varied in steps of 0.2 mm/μs until the minimum velocity for a shock-to-detonation transition was determined for each projectile diameter. Some one- and two-dimensional results are listed in Table 2, where ϕ is the projectile diameter in the case of two-dimensional computations and flyer plate thickness in the case of one-dimensional computations, V_* is the critical velocity, P_I the peak pressure of the initial shock pulse in the explosive, X_* the distance of shock run to detonation, T_* the time of run to detonatiion, and $V_*^2\phi$ is a parameter equivalent to the critical energy criterion. We also include the corresponding results p_i, x_*, and t_* obtained from the one-dimensional computation using SIN which produces the same critical velocities. Using the detonation pressure, P_{CJ} = 28.4 GPa, for composition-B, we have calculated the average rate of shock buildup Y_*, y_* and the gradient of shock buildup Z_*, z_* defined as follows:

$$Y_* = (P_{CJ} - P_I)/T_*,$$
$$y_* = (P_{CJ} - p_i)/t_*,$$
$$Z_* = (P_{CJ} - P_I)/X_*,$$
$$z_* = (P_{CJ} - p_i)/x_*.$$

It should be noted that conditions cited as critical in the table may be very close to critical or as much as 0.2 mm/μs above the cited value. Thus, our definition of critical values is not entirely uniform.

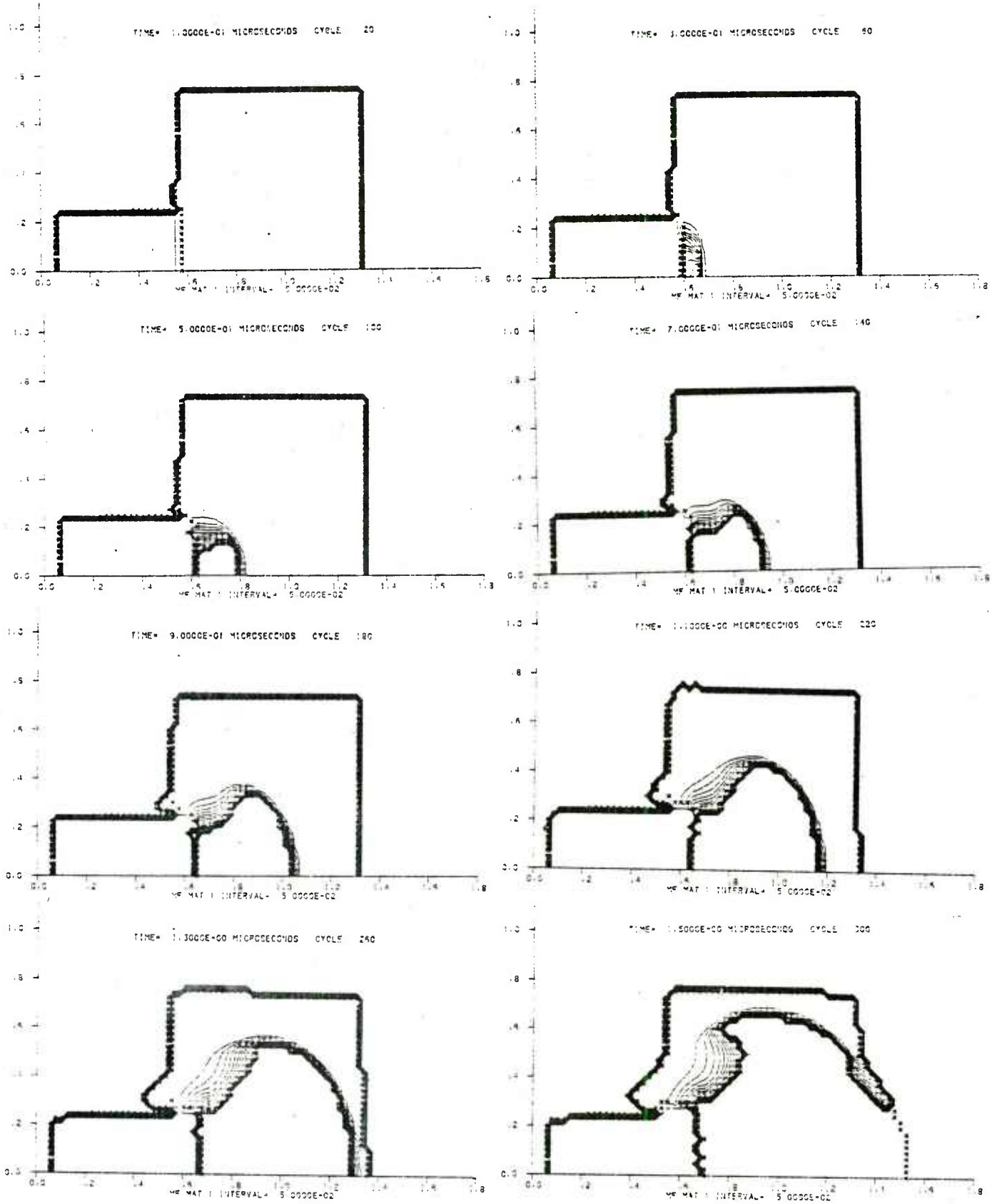

Figure 1a. Mass-Fraction Contours Showing the Spread of Reaction in Bare Charge (ϕ = 5 mm, V = 1.4 mm/μs).

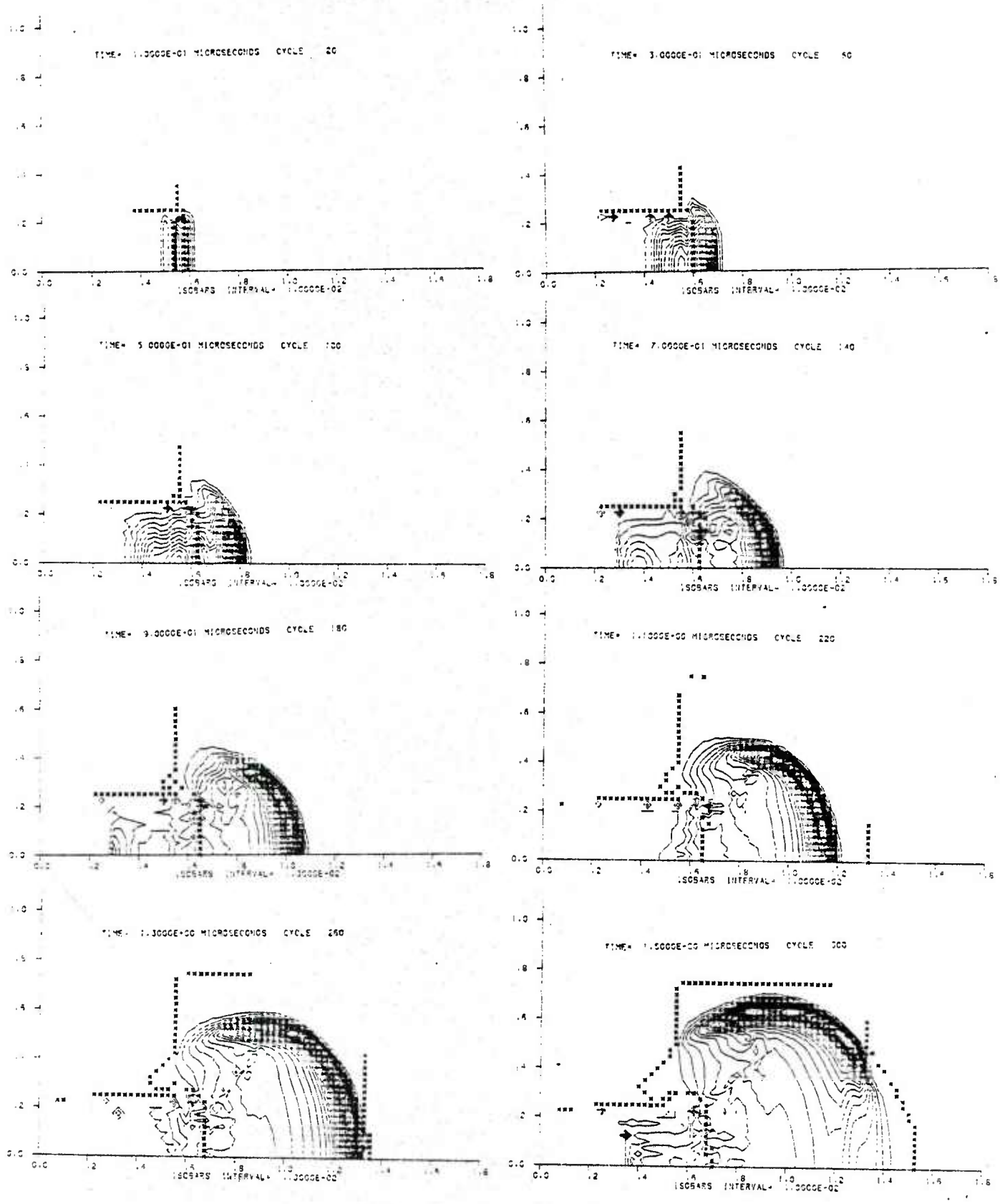

Figure 1b. Isobars Showing Shock and Reaction in Bare Charge (ϕ = 5 mm, V = 1.4 mm/μs).

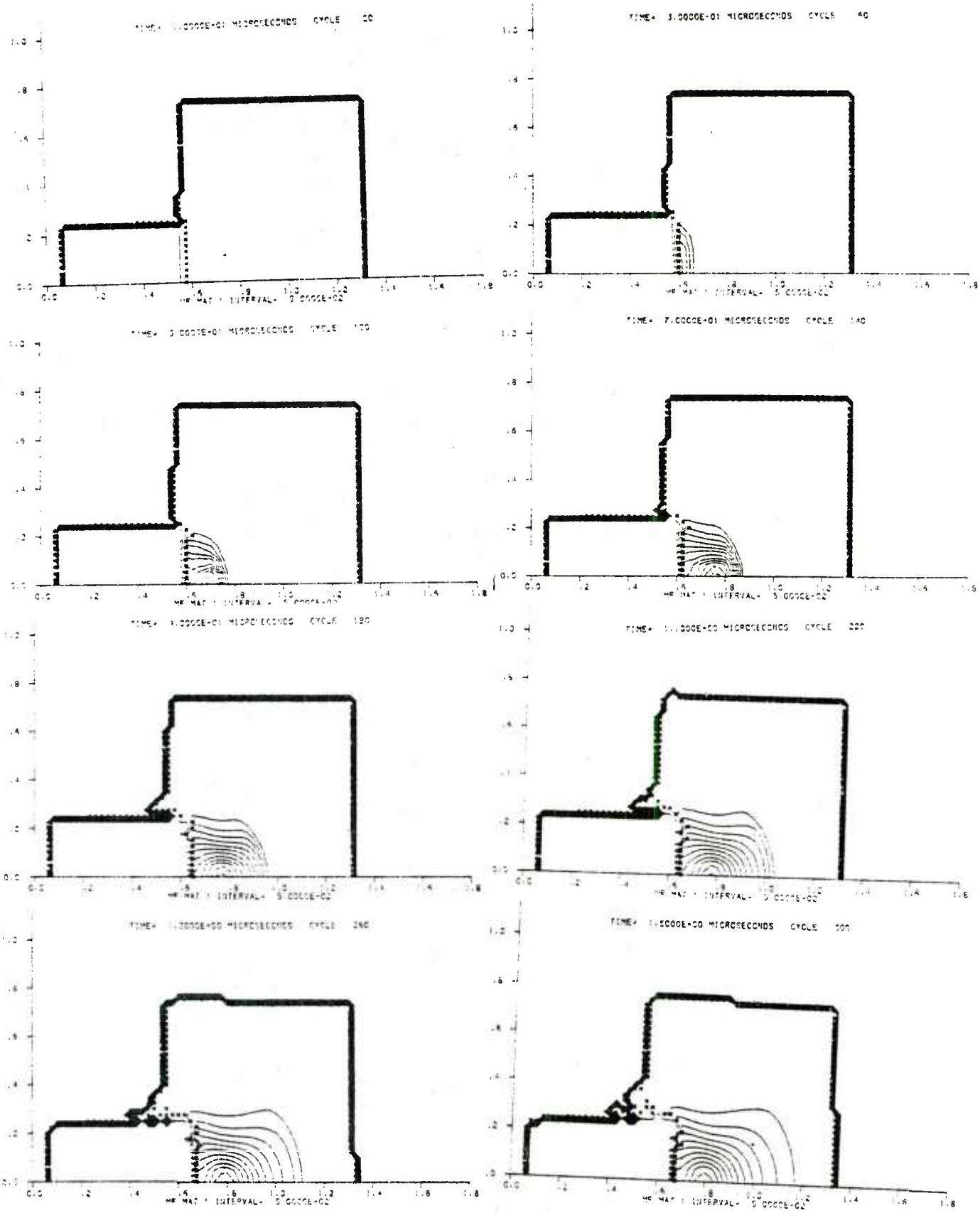

Figure 2a. Mass-Fraction Contours for "NO GO" in Bare Charge (ϕ = 5 mm, V = 1.2 mm/μs).

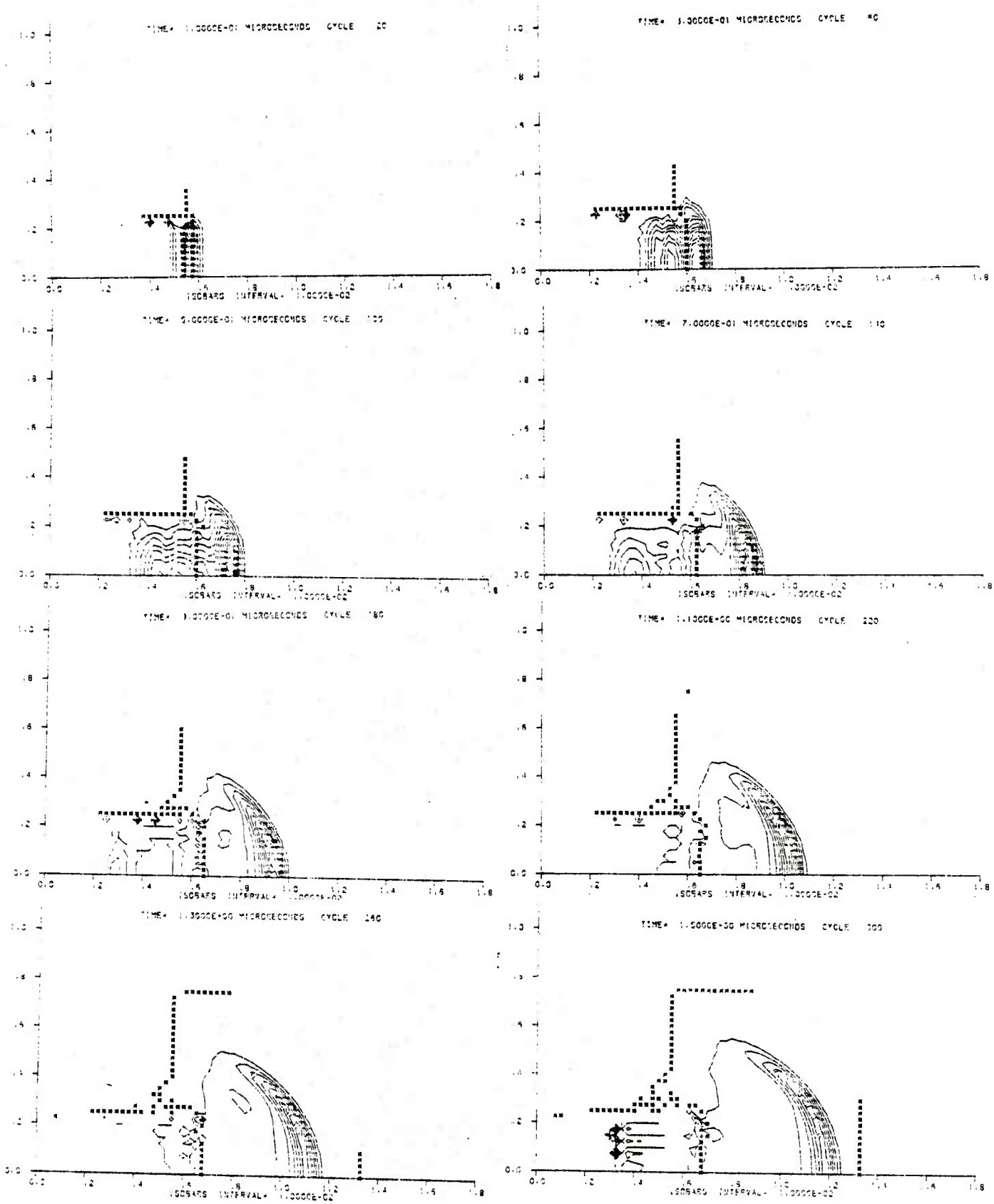

Figure 2b. Isobars for "NO GO" in Bare Charge
(ϕ = 5 mm, V = 1.2 mm/μs).

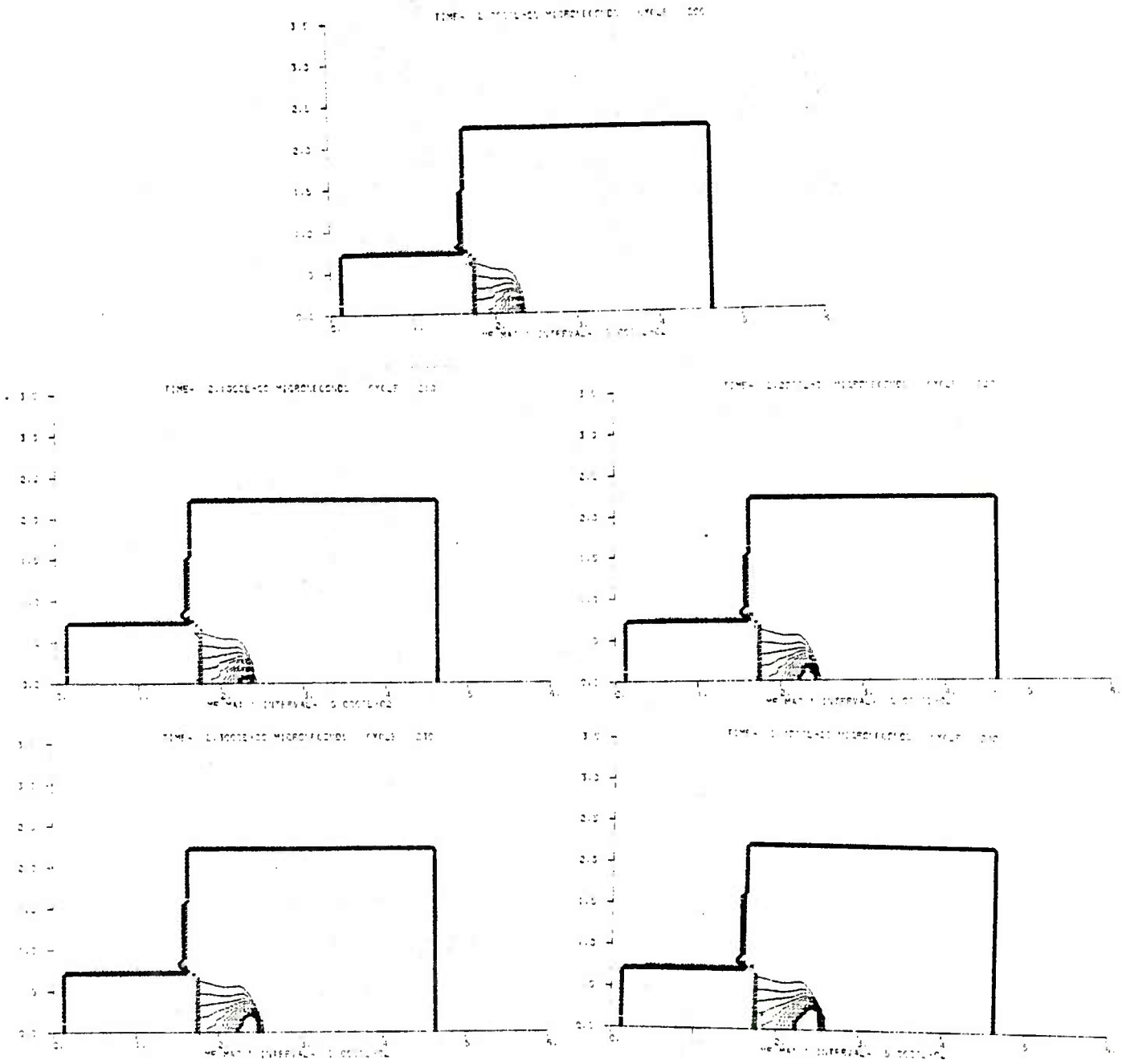

Figure 3. Mass-Fraction Contours Showing the Spread of Reaction in Bare Charge (ϕ = 15 mm, V = 0.7 mm/μs).

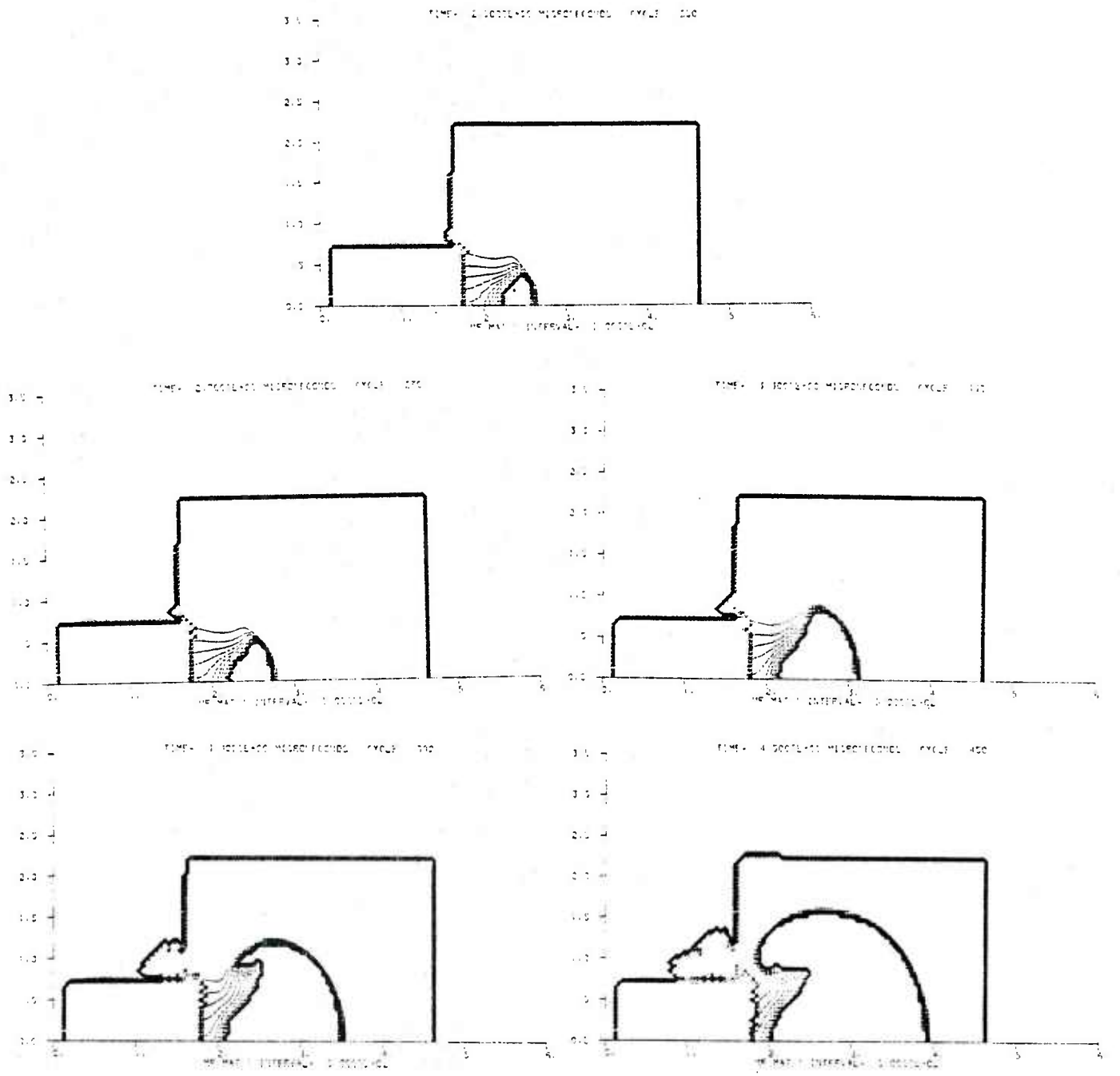

Figure 3. Mass-Fraction Contours (continued)

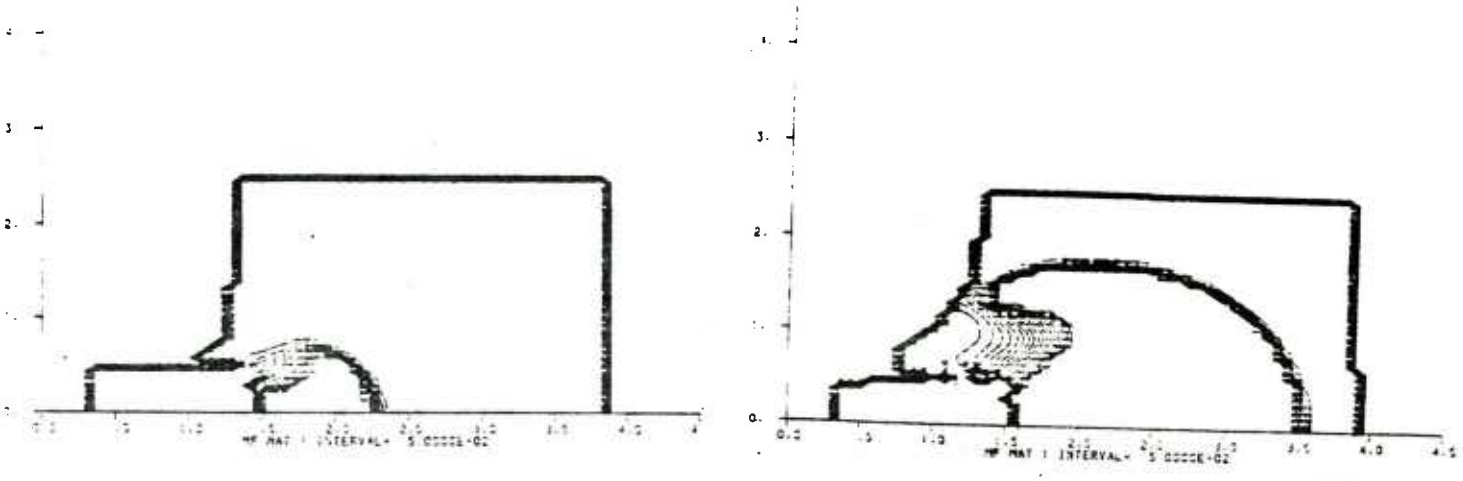

(a) Projectile with $\ell/\phi = 1.0$

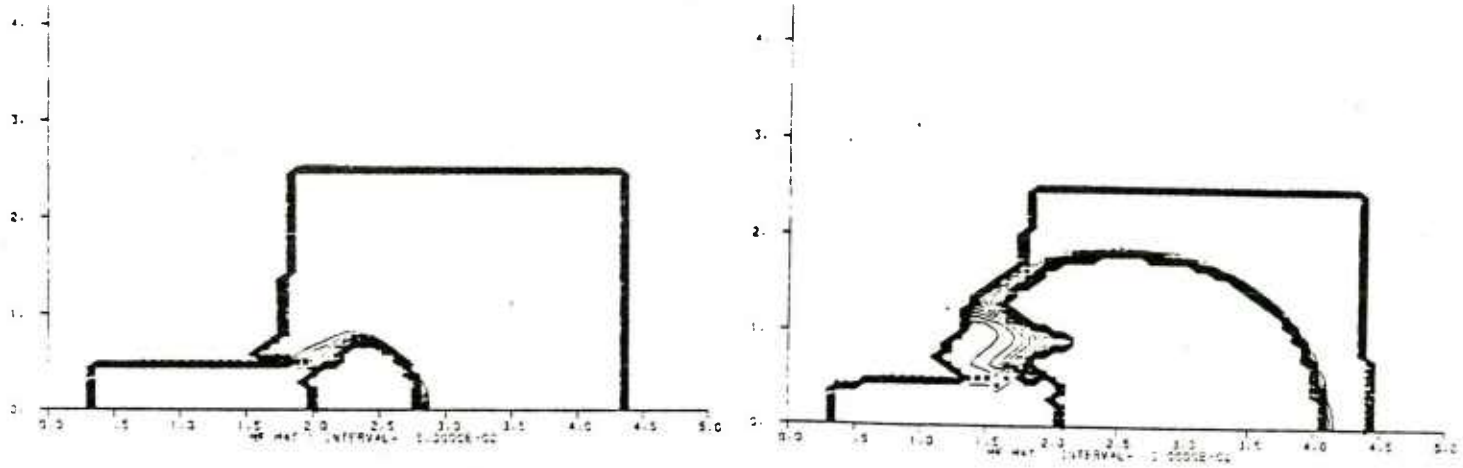

(b) Projectile with $\ell/\phi = 1.5$

Figure 4. Comparison of Different Aspect Ratios (ϕ = 10 mm, $V_* = 1.2$ mm/μs).

TABLE 2

Summary of Computed Critical Values - Bare Charges.

ϕ (mm)	V_* (mm/μs)	P_I (GPa)	X_* (mm)	T_* (μs)	Y_* (GPa/μs)	Z_* (GPa/mm)	$V_*^2\phi$ $mm^3/\mu s^2$	p_i (GPa)	x_* (mm)	t_* (μs)	y_* (GPa/μs)	z_* (GPa/mm
5	1.40	11.5	2.5	0.3	56.3^{D1}	6.76	9.80^{D1}	8.4	5.4	0.79	25.3^{D1}	3.70
8	1.00	6.4	3.8	0.9	24.4	5.79	8.00	5.2	9.3	1.63	14.2	2.49
10	0.90	5.8	12.5^{D2}	3.0^{D2}	7.5^{D2}	1.81^{D2}	8.10	4.4	11.3	2.12	11.3	2.12
12	0.80	4.8	6.8	1.7	13.9	3.47	7.68	4.0	12.5	2.38	10.2	1.95
15	0.70	3.8	9.0	2.3	10.7	2.73	7.35	3.4	15.3	3.13	8.0	1.63
18	0.60	2.8	13.0	3.2	8.0	1.97	6.48	3.0	17.3	3.62	7.0	1.47

D1 deviation from general trend of the column probably due to small ϕ.

D2 deviation from general trend of the column due to delayed initiation.

In Figure 5 we have plotted critical velocity obtained in our 2DE calculations versus the parameter $1/\sqrt{\phi}$ for comparison with the NOL empirical formula. Our computed critical velocities fall slightly below the experimental values but still exhibit the characteristic linear dependence on $1/\sqrt{\phi}$. The straight line of Figure 5 can be described by the equation:

$$V_* = a_1 + b_1 /\sqrt{\phi} \qquad (1)$$

with constants $a_1 = -0.16$ mm/μs and $b_1 = 3.33$ mm$^{3/2}$/μs. The critical velocity at $\phi = 5$ mm appears to deviate somewhat from the linear relation and has not been included in the fit. This is apparently a consequence of the alternate mode of buildup observed for the small-diameter high-velocity case. It may be noted that Equation (1) has been used for a long time. (Note $a_1 = 0$ and $b_1 = 3.26$ mm$^{3/2}$/μs for composition-B in Reference 1.)

As previously noted, our cited critical conditions vary from the actual conditions in a nonuniform manner. It is of interest to observe how closely the paths to initiation conform to the Pop-plot for comp-B. This is illustrated in Figure 6. The SIN results are all seen to lie reasonably close to the Pop-plot indicating that the single-curve buildup hypothesis (implied in Forest Fire) is applicable to the one-dimensional situation. However, for the multidimensional projectile impact case buildup deviates considerably from the Pop-plot. This appears to be chiefly due to the near critical nature of the cases considered while the Pop-plot represents supercritical buildup. For example, the computation at $\phi = 10$ mm almost doesn't initiate. The pressure first builds, then drops off and finally rises again to the CJ value. This is clearly our most nearly critical case. The computation at $\phi = 8$ mm is more supercritical and conforms more exactly to the Pop-plot. Only one point could be obtained at $\phi = 10$ mm. This point lies below the Pop-plot while the results at larger diameters were generally above the Pop-plot. This gives a third indication that the buildup to detonation proceeds somewhat differently in the small-diameter, high-velocity case.

In the literature, the critical energy criterion [7] has been very popular for the study of one-dimensional shock initiation (as in the wedge test). If this criterion is applicable to our two-dimensional study, then we must have $V_*^2 \phi = \text{constant}$. Yet our numerical results of Table 2 do not maintain a strict constancy of $V_*^2 \phi$. However, some of this may be explained by the nonuniform determination of the critical condition .

In the original derivation of the critical energy criterion, the shape and width of the initial shock pulse play an important role in characterizing the shock initiation. In our

7. *F. E. Walker and R. J. Wasley," Critical Energy for Shock Initiation of Heterogeneous Explosives," Explosivstoffe Nr. 1, 1969, pp 9-13.*

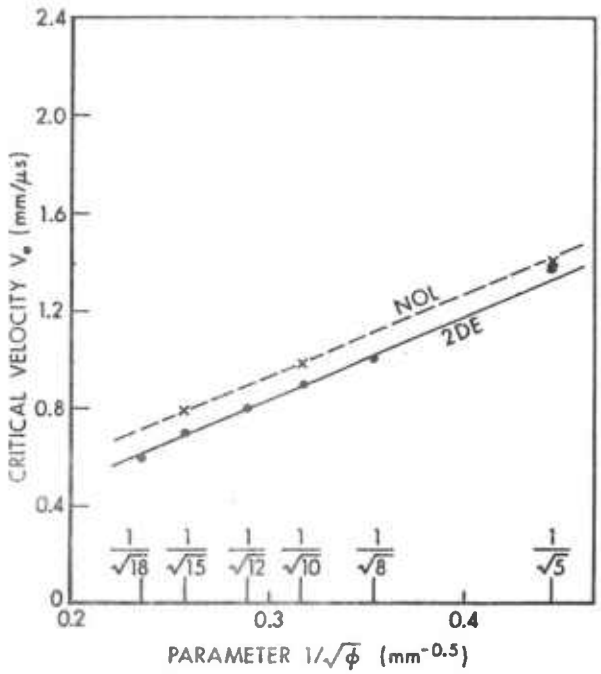

Figure 5. Critical Velocity vs $1/\sqrt{\phi}$ for Bare Explosive Charges.

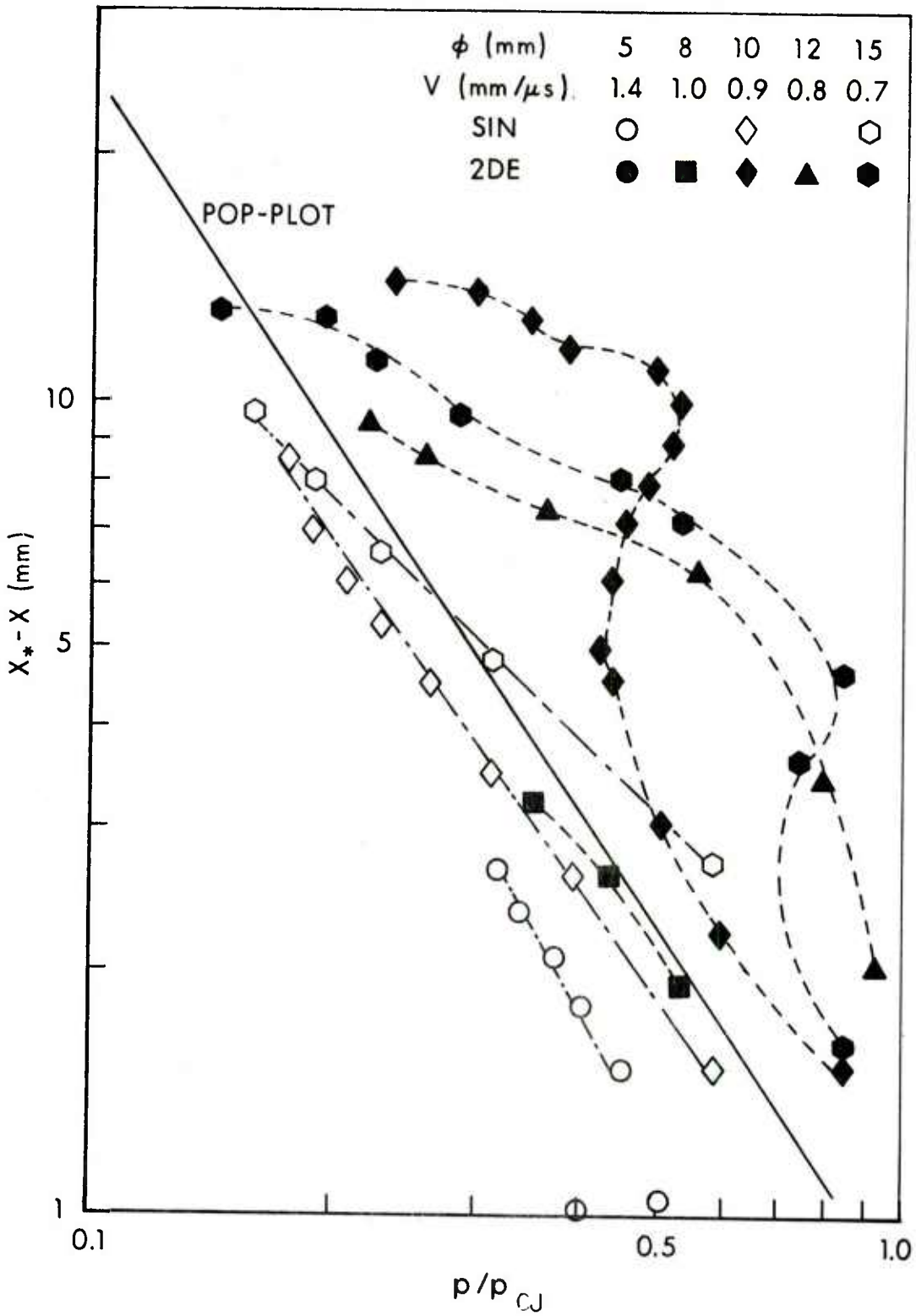

Figure 6. Comparison of Shock Buildup Trajectories to Pop-Plot.

two-dimensional impact problem, the pulse shape and duration are affected by rarefaction waves issuing from free surfaces and edges. It appears, however, that the reactive shock in the explosive can accelerate to detonation by self-support provided the necessary conditions are satisfied. A number of other linear relations among the problem parameters were observed as illustrated in Figures 7-11. The following linear fits can serve to complement Equation (1) and provide a full description of the initiation process in terms of the stimulus.

$$P_I = a_2 + b_2 V_* = a_2' + b_2'/\sqrt{\phi} \tag{2}$$

$$T_* = a_3 + b_3 \phi \tag{3}$$

$$X_* = a_4 + b_4 T_* \tag{4}$$

$$Y_* = a_5 + b_5 V_* = a_5' + b_5'/\sqrt{\phi} \tag{5}$$

$$Z_* = a_6 + b_6 V_* = a_6' + b_6'/\sqrt{\phi} \tag{6}$$

The values of the constants are given in Table 3. It should be noted that Equation (4) represents a relationship that is a property of the explosive only. The foregoing linear relations also appear to hold good for our SIN results. In fact, the SIN results fit straight lines even better in Figures 7-11.

III. SHOCK INITIATION OF COVERED EXPLOSIVE CHARGES

We have also addressed the related problem posed by introducing a steel plate of thickness h between the steel projectile and the composition-B. Table 4 summarizes our new grids. We have considered projectile diameters of 5,8,10,12 and 15 mm and cover plates of one-third and one-half the diameter in each case.

Detonation in the covered charges develops in a manner similar to the bare charges as illustrated in the mass-fraction contour plots of Figure 12 for a 15 mm projectile with an impact velocity of 1.0 mm/μs.

The critical parameter-values are summarized in Table 5. For $h/\phi = 1/3$, the critical energy criterion ($V_*^2 \phi = \text{Const}$) is followed almost exactly except in the 5 mm diameter case. The constancy of $V_*^2\phi$, is also good for $h/\phi = 1/2$.

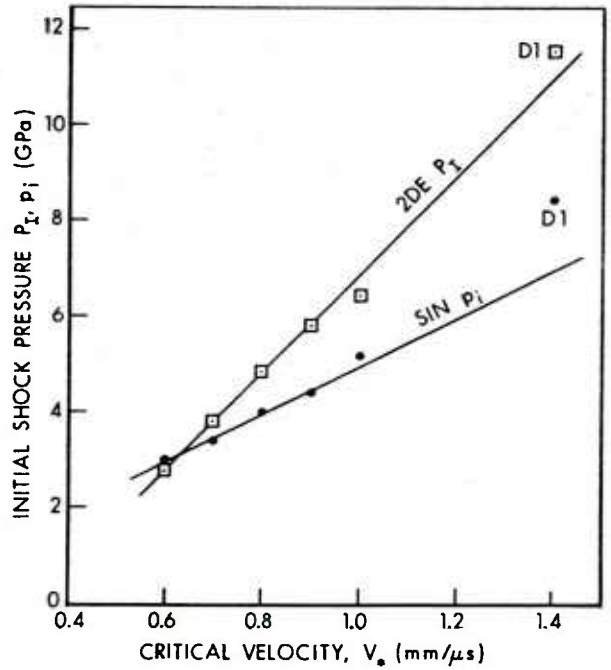

(a) Initial Shock Pressure versus Critical Velocity.

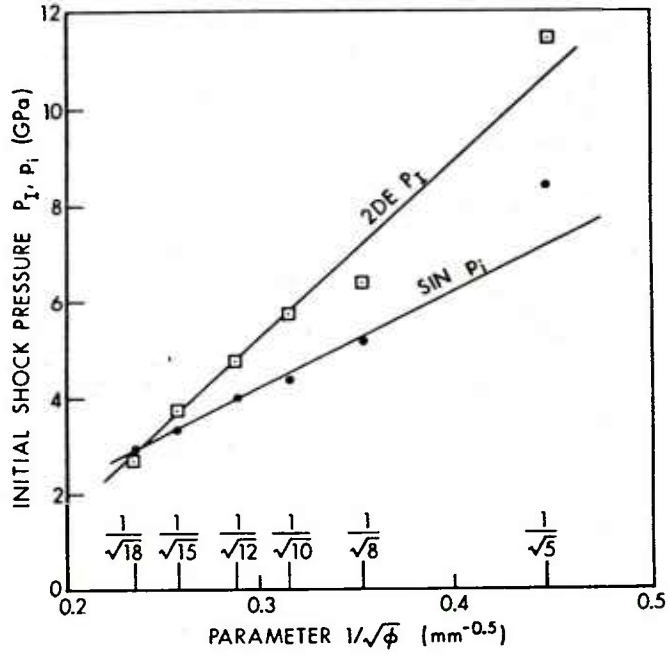

(b) Initial Shock Pressure versus $1/\sqrt{\phi}$.

Figure 7. Linear Fits of Initial Shock Pressure.

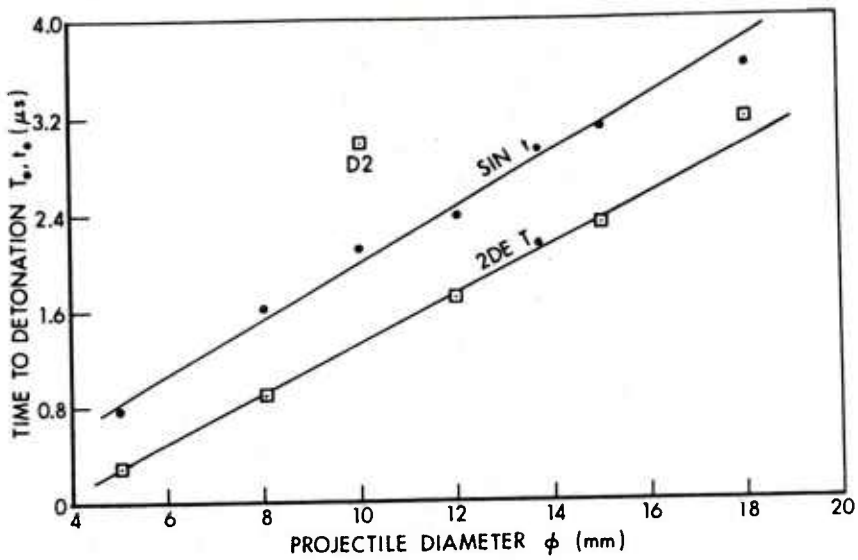

Figure 8. Linear Fit of Time to Detonation versus Projectile Diameter.

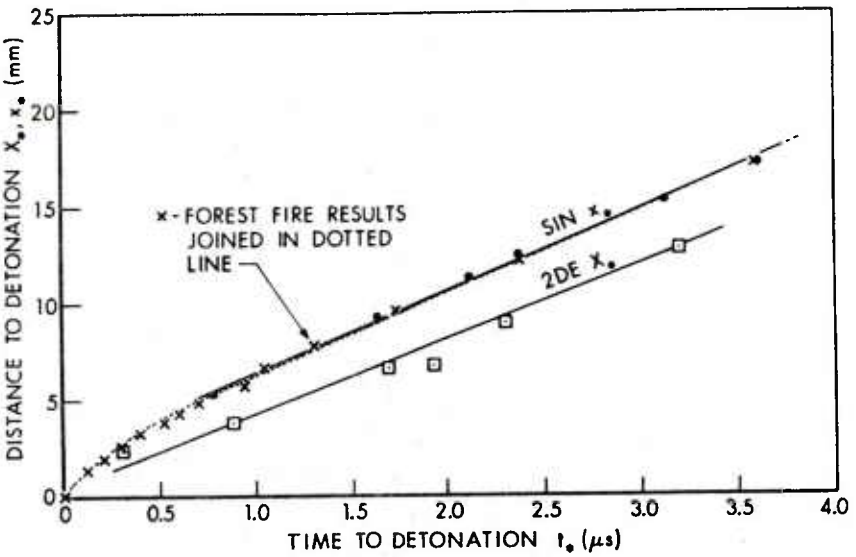

Figure 9. Linear Fit of Distance to Detonation versus Time to Detonation.

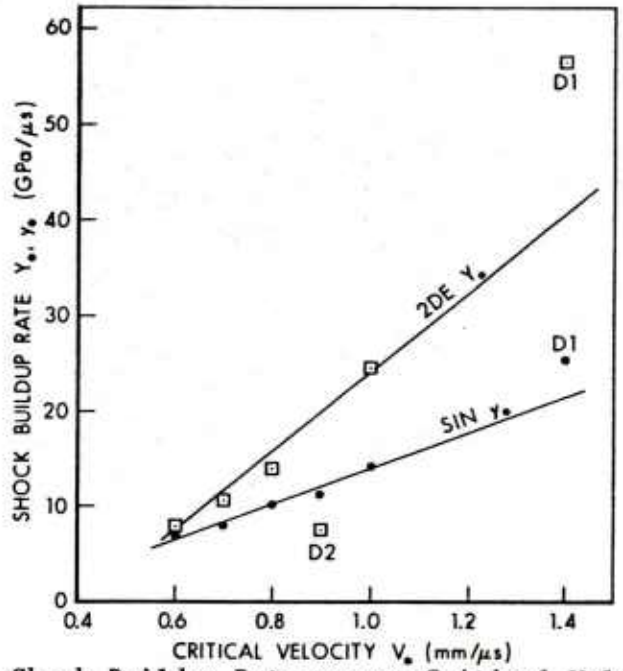

(a) Shock Buildup Rate versus Critical Velocity.

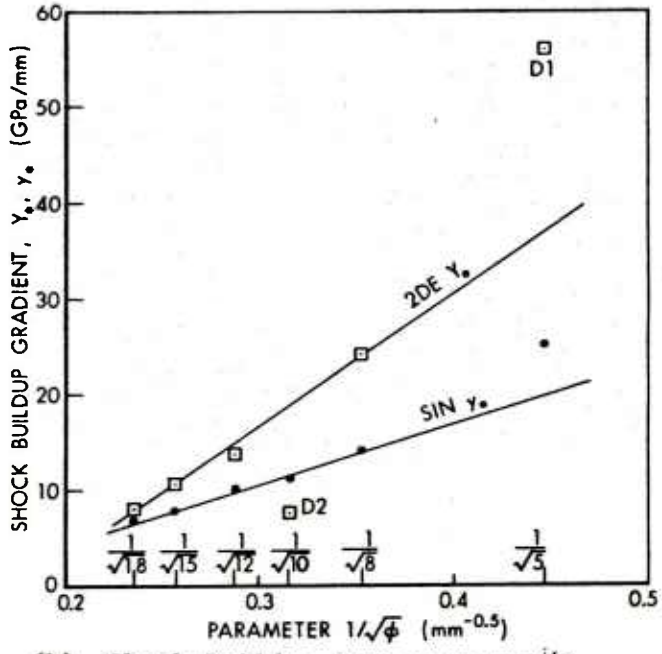

(b) Shock Buildup Rate versus $1/\sqrt{\phi}$

Figure 10. Linear Fits of Shock Buildup Rate.

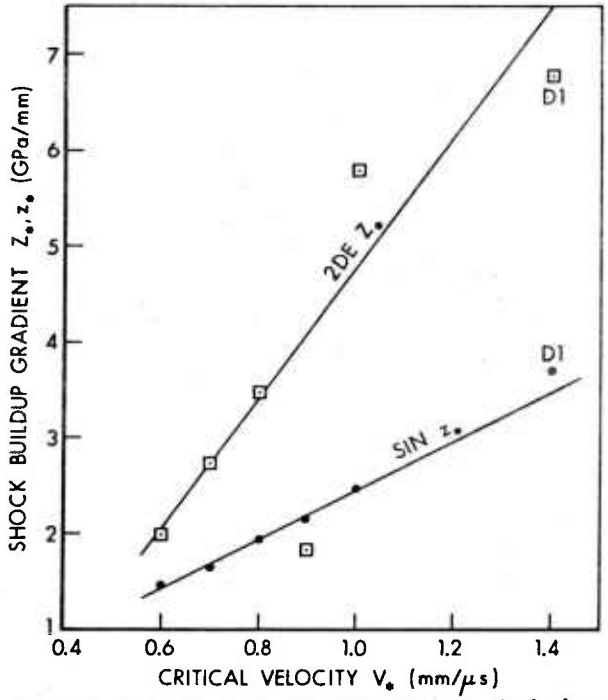

(a) Shock Buildup Gradient versus Critical Velocity

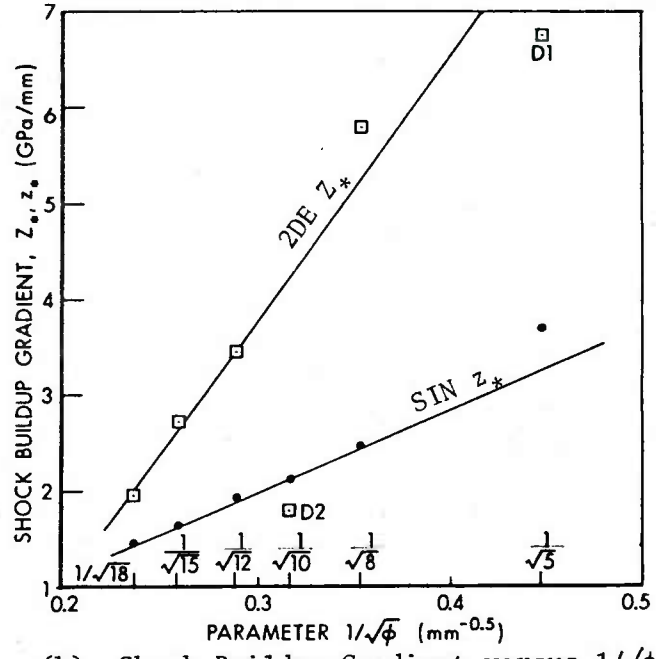

(b) Shock Buildup Gradient versus $1/\sqrt{\phi}$.

Figure 11. Linear Fits of Shock Buildup Gradient.

TABLE 3

Constants a_i and b_i of Equation (i), i = 1-6.

	i = 1		i = 2		i = 3		i = 4		i = 5		i = 6	
	SIN	2DE	SIN	2DE	SIN	2DE	SIN	2DE	SIN	2DE	SIN	2DE
a_i	-0.16	-0.16	-0.1	-3.2	-0.35	-0.81	2.19	0.39	-4.88	-17.0	-0.05	-2.09
b_i	3.33	3.33	5.0	10.0	0.23	0.21	4.23	3.89	18.75	40.9	2.50	6.88

For units of a_i and b_i see Equation (1) - (6).

TABLE 4

Input Data For 2DE Computational Grids - Covered Charges

h/ϕ	ϕ (mm)	ΔR (mm)	I	ΔZ (mm)	J	ΔT (μs)	N
	5	0.125	45	0.125	125	0.0025	1,000
	8	0.200	45	0.200	125	0.0050	900
1/3	10	0.250	45	0.250	125	0.0050	900
	12	0.240	55	0.240	140	0.0050	900
	15	0.300	55	0.300	140	0.0080	700
	5	0.125	45	0.125	140	0.0025	1,000
	8	0.200	45	0.200	125	0.0050	1,000
1/2	10	0.250	45	0.250	125	0.0050	800
	12	0.240	55	0.240	140	0.0050	1,000
	15	0.300	55	0.300	140	0.0080	700

TABLE 5

Summary of Computed Critical Values - Covered Charges

h/ϕ	ϕ (mm)	V (mm/μs)	$V_*^2\phi$ ($mm^3/\mu s^2$)	P_I (GPa)	X_* (mm)	T_* (μs)	Y_* (GPa/μs)	Z_* (GPa/mm)
	5	1.4	9.80	10.0	1.13	0.24	76.6	16.3
	8	1.2	12.10	10.0	1.8	0.35	52.6	10.2
1/3	10	1.1	12.10	10.0	2.3	0.50	36.8	8.0
	12	1.0	12.00	8.0	2.5	0.06	34.0	8.1
	15	0.9	12.15	7.0	3.6	0.90	23.8	5.9
	5	1.7	14.45	14.0	0.63	0.1	144.0	22.9
	8	1.4	15.60	14.0	0.8	0.3	48.0	18.0
1/2	10	1.3	15.90	12.0	1.0	0.3	54.7	16.4
	12	1.2	16.15	11.0	2.3	0.4	43.5	7.6
	15	1.0	15.00	10.0	3.6	1.0	18.4	5.1

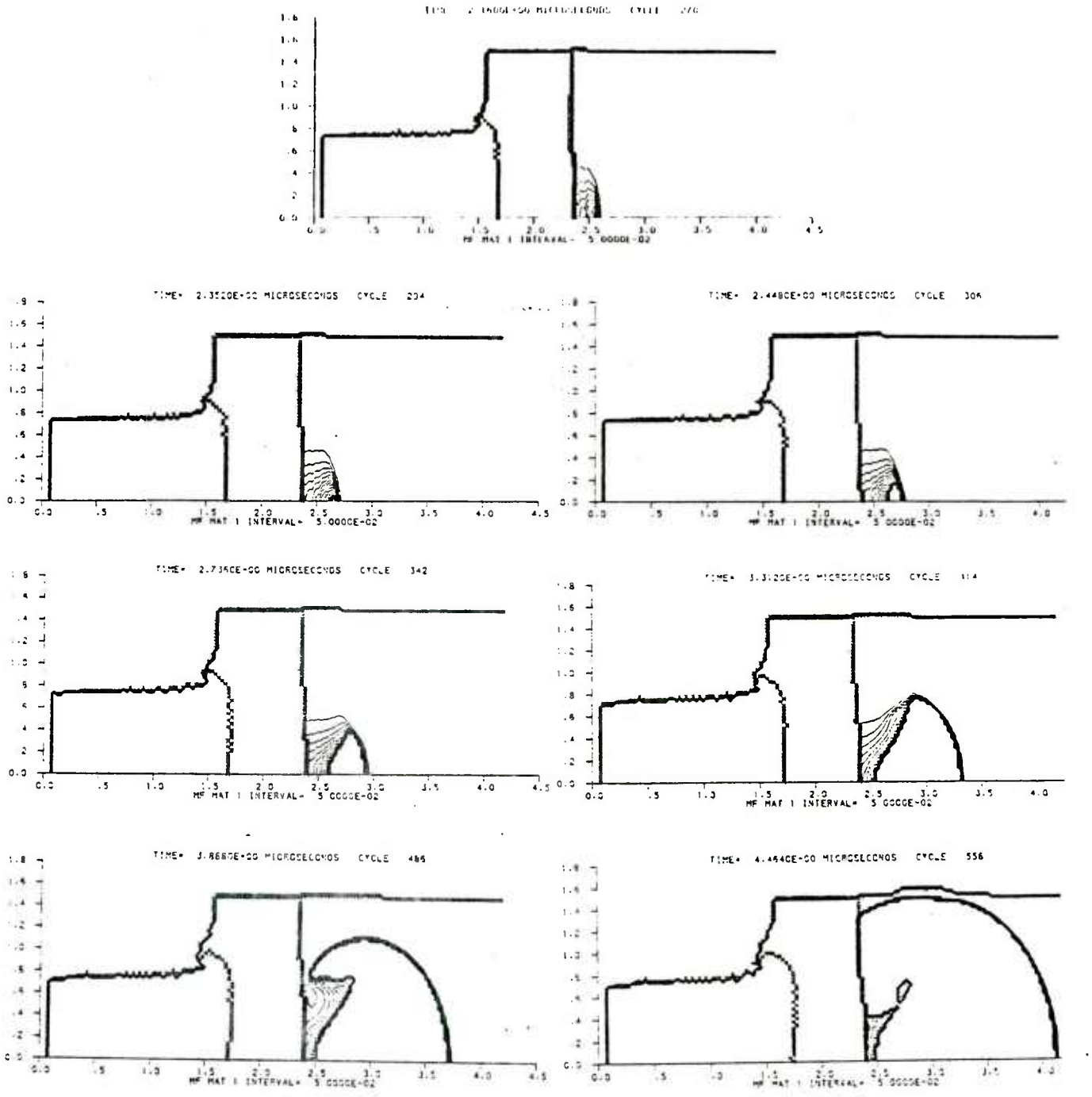

Figure 12. Mass-Fraction Contours Showing the Spread of Reaction in Covered Charge (ϕ = 15 mm, h/ϕ = 1/2, V - 1/0 mm/μs, GO).

The Jacobs-Roslund (NOL) formula[3] for normal impact against covered charges may be written

$$V_*' = V_* (1 + h/\phi)^{-1} = V_o + A/\sqrt{\phi} \qquad (7)$$

Plotting V_*' versus $1/\sqrt{\phi}$, as in Figure 13, allows a comparison of the computed results at $h/\phi = 0, 1/3$ and $1/2$ with the results of the Jacobs-Roslund formulas with $V_o = 0$ and $A = 3.13$ mm $^{3/2}/\mu s$. Only at the smaller projectile diameter do the results for the covered charges differ significantly from the linear relationships defined by the bare charge results. In addition, the covered charge results tend to diverge from one another at smaller diameters.

Plots corresponding to those of Figures 7-11 for the bare charge problem have also been constructed in the covered charge case. These are shown in Figures 14-17. Figure 16, which corresponds to Figure 9, shows the distance to detonation plotted versus the time to detonation. As previously noted, this is strictly an explosive property according to the single-curve buildup hypothesis and should be independent of h/ϕ.

IV. SUMMARY

Using the SIN and 2DE hydrodynamic computer codes, we have conducted a numerical study of the shock initiation response of both bare and covered composition-B charges to projectile impact.

In the bare charge case we observed two modes of shock initiation. In the case of larger projectile diameters, the detonation is observed to begin at some distance from the impact point and propagate outward. When the projectile diameter is sufficiently small (and the critical velocity correspondingly large) detonation occurs almost immediately. We also verified the independence of the shock initiation response with respect to projectile aspect ratio. We then determined critical conditions for shock initiation for six different projectile diameters with unit aspect ratio. Except for the case of the smallest projectile (ϕ= 5 mm), the critical velocity was observed to have a linear dependence on $1/\sqrt{\phi}$ with values falling a little below the NOL empirical line. The progress of buildup to detonation was observed and found to closely follow the Pop-plot when the impact was sufficiently supercritical. Finally, we generated additional linear relations to completely describe buildup to detonation in the critical case.

In the case of covered charges, we found that the development of detonation is similar to that observed for bare charges. Critical velocities and other parameters were determined as for the bare charges. The critical velocities, when adjusted for cover plate thickness according to the Jacobs-Roslund formula, were found to agree well with the bare charge results at larger

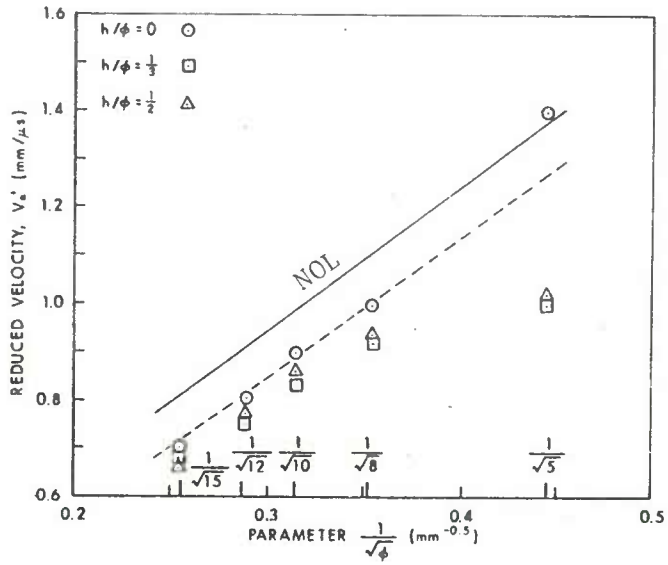

Figure 13. Comparison of Bare and Covered Charge Critical Velocity with Jacobs-Roslund Formula.

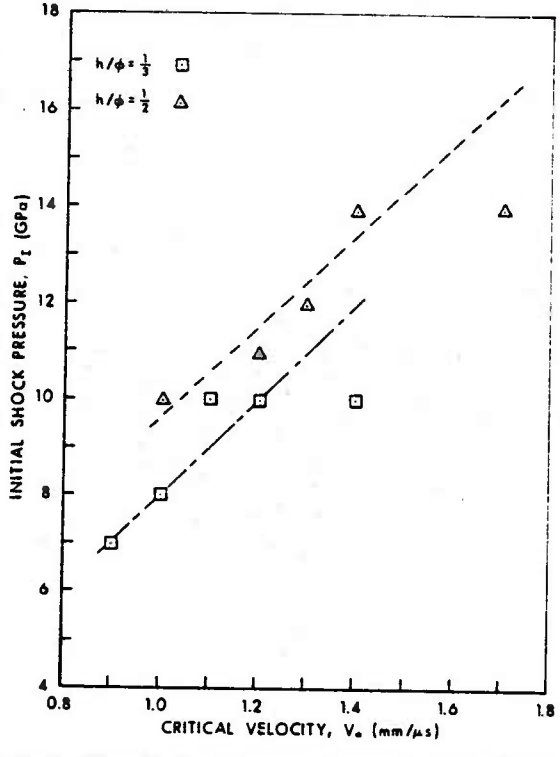

(a) Initial Shock Pressure versus Critical Velocity

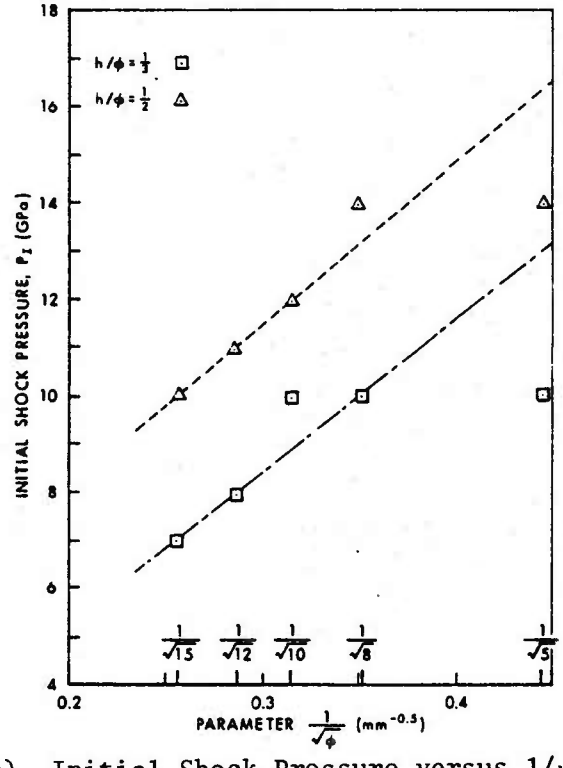

(b) Initial Shock Pressure versus $1/\sqrt{\phi}$.

Figure 14. Linear Fits of Initial Shock Pressure.

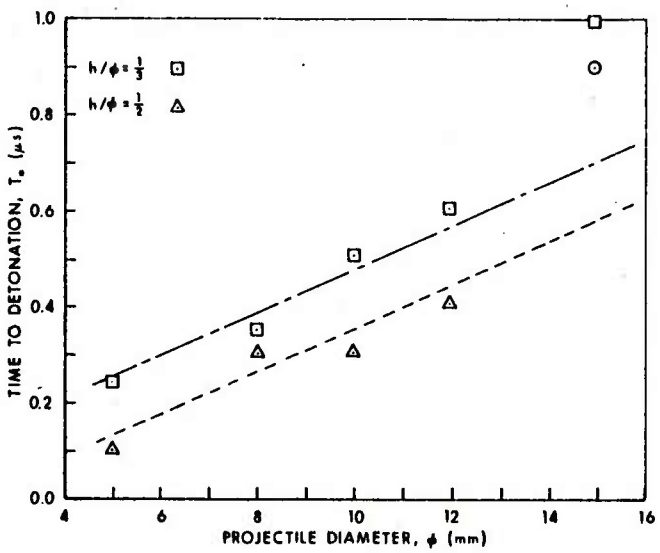

Figure 15. Linear Fit of Time to Detonation versus Projectile Diameter.

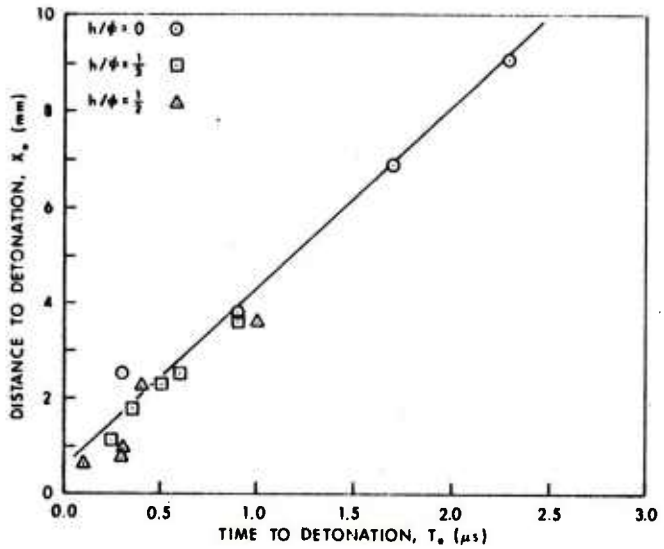

Figure 16. Linear Fit of Distance to Detonation versus Time to Detonation.

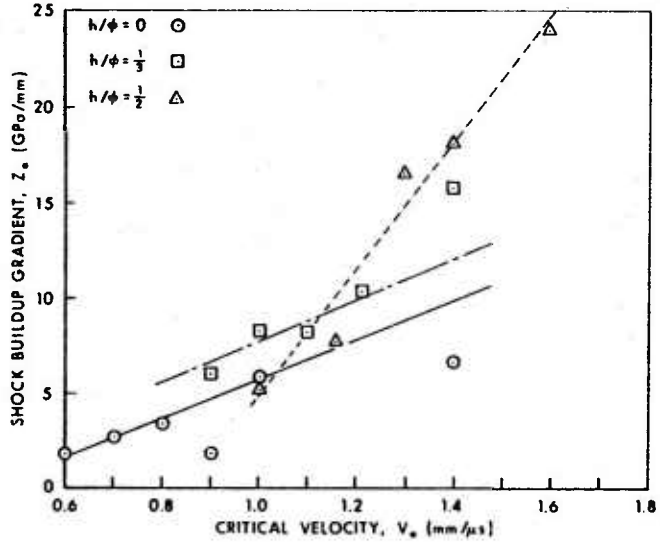

(a) Shock Buildup Gradient versus Critical Velocity

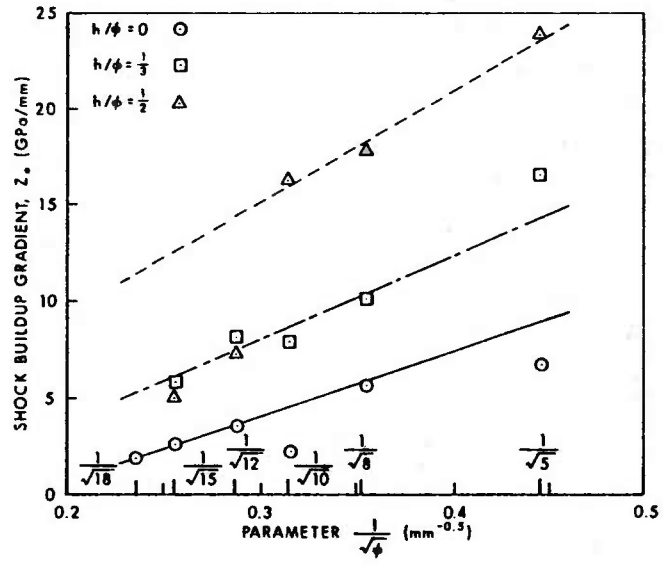

(b) Shock Buildup Gradient versus $1/\sqrt{\phi}$

Figure 17. Linear Fits of Shock Buildup Gradient.

projectile diameters and to diverge from the bare charge results and from each other with decreasing projectile diameter.

REFERENCES

1. D. C. Slade and J. Dewey, "High-Order Initiation of Two Military Explosives by Projectile Impact," Ballistic Research Laboratory Report No. 1021, July 1957 (AD 145868).

2. S. M. Brown and E. G. Whitbread, " The Initiation of Detonation by Shock Waves of Known Duration and Intensity, " Les Ondes De Detonation, C.N.R.S. No. 109 (Paris, 1962), pp 69-80.

3. L. A. Roslund, J. W. Watt, and N. L. Coleburn, "Initiation of Warhead Explosives by the Impact of Controlled Fragments I. Normal Impact," Naval Ordnance Laboratory Technical Report NOLTR-73-124, August 1974.

4. K. L. Bahl, H. C. Vantine and R. C. Wllingort, "The Shock Initiation of Bare and Covered Explosives by Projectile Impact," Seventh Symposium (International) on Detonation, June 1981, pp 325-335.

5. C. L. Mader and M. S. Shaw, "Users Manual for SIN, A One-Dimensional Hydrodynamic Code for Problems Which Include Chemical Reactions, Elastic Plastic Flow, Spalling Phase Transitions, Melting, Forest Fire, Detonation Buildup, and SESAME Tabular Equation of State," Los Alamos Scientific Laboratory Report LA-7264-M, September 1978.

6. J. D. Kershner and C. L. Mader, "2DE, A Two Dimensional Continuous Eulerian Hydrodynamic Code for Computing Multicomponent Reactive Hydrodynamic Problems," Los Alamos Scientific Laboratory Report LA-4846, March 1972.

7. F. E. Walker and R. J. Wasley, "Critical Energy for Shock Initiation of Heterogeneous Explosives," Explosivstoffe Mr. 1, 1969, pp 9-13.

DISTRIBUTION LIST

No. of Copies	Organization
12	Administrator Defense Technical Info Center ATTN: DTIC-DDA Cameron Station Alexandria, VA 22314
1	Chairman DOD Explosives Safety Board ATTN: Dr. T. Zaker Room 856-C Hoffman Bldg I 2461 Eisenhower Avenue Alexandria, VA 22331
1	Commander US Army Materiel Development and Readiness Command ATTN: DRCDMD-ST 5001 Eisenhower Avenue Alexandria, VA 22333
6	Commander US Army Armament Research and Development Command ATTN: DRDAR-TDC DRDAR-TSS DRDAR-LCE, Dr. R.F.Walker DRDAR-LCE, Dr. N. Slagg DRDAR-LCN, Dr. P. Harris Dover, NJ 07801
1	Commander US Army Armament Research and Development Command ATTN: DRSAR-LEP-L Rock Island, IL 61299
1	Director US Army ARRADCOM Benet Weapons Laboratory ATTN: DRDAR-LCB-TL Watervliet, NY 12189
1	Commander US Army Aviation Research and Development Command ATTN: DRDAV-E 4300 Goodfellow Boulevard St. Louis, MO 63120
1	Director US Army Air Mobility Research and Development Laboratory Ames Research Center Moffett Field, CA 94035
1	Commander US Army Communications Rsch and Development Command ATTN: DRSEL-ATDD Fort Monmouth, NJ 07703
1	Commander US Army Electronics Research and Development Command Technical Support Activity ATTN: DELSD-L Fort Monmouth, NJ 07703
1	Commander US Army Missile Command ATTN: DRSMI-R Redstone Arsenal, AL 35898
1	Commander US Army Missile Command ATTN: DRSMI-YDL Redstone Arsenal, AL 35898
1	Commander US Army Missile Command ATTN: DRSME-RK, Dr. R. G. Rhoades Redstone Arsenal, AL 35898
1	Commander US Army Tank Automotive Command ATTN: DRSTA-TSL Warren, MI 48090

DISTRIBUTION LIST

No. of Copies	Organization
1	Director US Army TRADOC Systems Analysis Activity ATTN: ATAA-SL White Sands Missile Range NM 88002
2	Commandant US Army Infantry School ATTN: ATSH-CD-CSO-OR Fort Benning, GA 31905
1	Commander US Army Research Office ATTN: Chemistry Division P.O. Box 12211 Research Triangle Park, NC 27709
1	Commander Office of Naval Research ATTN: Dr. J. Enig, Code 200B 800 N. Quincy Street Arlington, VA 22217
1	Commander Naval Sea Systems Command ATTN: Mr. R. Beauregard, SEA 64E Washington, DC 20360
1	Commander Naval Explosive Ordnance Disposal Facility ATTN: Technical Library Code 604 Indian Head, MD 20640
1	Commander Naval Research Lab ATTN: Code 6100 Washington, DC 20375
1	Commander Naval Surface Weapons Center ATTN: Code G13 Dahlgren, VA 22448
9	Commander Naval Surface Weapons Center ATTN: Mr. L. Roslund, R122 Mr. M. Stosz, R121 Code X211, Lib E. Zimet, R13 R.R. Bernecker, R13 J.W. Forbes, R13 S.J. Jacobs, R10 K. Kim, R13 Dr. C. Dickinson Silver Spring, MD 20910
4	Commander Naval Weapons Center ATTN: Dr. L. Smith, Code 3205 Dr. A. Amster, Code 385 Dr. R. Reed, Jr., Code 388 Dr. K. J. Graham, Code 3835 China Lake, CA 93555
1	Commander Naval Weapons Station NEDED ATTN: L. Rothstein, Code 50A Yorktown, VA 23691
1	Commander Fleet Marine Force, Atlantic ATTN: G-4 (NSAP) Norfolk, VA 23511
1	Commander AFRPL ATTN: Mr. R. Geisler, Code AFRPL MKPA Edwards AFB, CA 93523
1	AFWL/SUL Kirtland AFB, NM 87117
1	Director US Army BMD Advanced Technology Center ATTN: Dr. David C. Sayles P. O. Box 1500 Huntsville, AL 35807

DISTRIBUTION LIST

No. of Copies	Organization
1	Director Lawrence Livermore Laboratory University of California ATTN: Dr. M. Finger P.O. Box 808 Livermore, CA 94550
1	Director Los Alamos Scientific Laboratory ATTN: John Ramsay P.O. Box 1663 Los Alamos, NM 87544
1	Director Sandia National Laboratory ATTN: Dr. J. Kennedy Albuquerque, NM 87115

Aberdeen Proving Ground

Dir, USAMSAA
ATTN: DRXSY-D
DRXSY-MP, H. Cohen

Cdr, USATECOM
ATTN: DRSTE-TO-F

Dir, USACSL
ATTN: DRDAR-CLB-PA
DRDAR-CLN
DRDAR-CLJ-L

USER EVALUATION OF REPORT

Please take a few minutes to answer the questions below; tear out this sheet, fold as indicated, staple or tape closed, and place in the mail. Your comments will provide us with information for improving future reports.

1. BRL Report Number _____

2. Does this report satisfy a need? (Comment on purpose, related project, or other area of interest for which report will be used.)

_____

_____

_____

3. How, specifically, is the report being used? (Information source, design data or procedure, management procedure, source of ideas, etc.) _____

_____

_____

4. Has the information in this report led to any quantitative savings as far as man-hours/contract dollars saved, operating costs avoided, efficiencies achieved, etc.? If so, please elaborate.

_____

_____

5. General Comments (Indicate what you think should be changed to make this report and future reports of this type more responsive to your needs, more usable, improve readability, etc.) _____

_____

_____

_____

6. If you would like to be contacted by the personnel who prepared this report to raise specific questions or discuss the topic, please fill in the following information.

Name: _____

Telephone Number: _____

Organization Address: _____

_____

_____